

Chemical Science

Accepted Manuscript



This is an *Accepted Manuscript*, which has been through the Royal Society of Chemistry peer review process and has been accepted for publication.

Accepted Manuscripts are published online shortly after acceptance, before technical editing, formatting and proof reading. Using this free service, authors can make their results available to the community, in citable form, before we publish the edited article. We will replace this *Accepted Manuscript* with the edited and formatted *Advance Article* as soon as it is available.

You can find more information about *Accepted Manuscripts* in the [Information for Authors](#).

Please note that technical editing may introduce minor changes to the text and/or graphics, which may alter content. The journal's standard [Terms & Conditions](#) and the [Ethical guidelines](#) still apply. In no event shall the Royal Society of Chemistry be held responsible for any errors or omissions in this *Accepted Manuscript* or any consequences arising from the use of any information it contains.



www.rsc.org/chemicalscience

ARTICLE

Base catalytic activity of alkaline earth MOFs: a (micro)spectroscopic study of active site formation by controlled transformation of structural anions

Cite this: DOI: 10.1039/x0xx00000x

Received 00th January 2012,
Accepted 00th January 2012

DOI: 10.1039/x0xx00000x

www.rsc.org/P. Valvekens,^a D. Jonckheere,^a T. De Baerdemaeker,^a A. V. Kubarev,^a M. Vandichel,^b K. Hemelsoet,^b M. Waroquier,^b V. Van Speybroeck,^b E. Smolders,^c D. Depla,^d M.B.J. Roeffaers,^a D. De Vos^{a*}

A new concept has been developed for generating highly dispersed base sites on metal-organic framework (MOF) lattices. The base catalytic activity of two alkaline earth MOFs, $M_2(\text{BTC})(\text{NO}_3)(\text{DMF})$ ($M = \text{Ba}$ or Sr , $\text{H}_3\text{BTC} = 1,3,5\text{-benzenetricarboxylic acid}$, $\text{DMF} = N,N\text{-dimethylformamide}$) was studied as a function of their activation procedure. The catalytic activity in Knoevenagel condensation and Michael addition reactions was found to increase strongly with activation temperature. Physicochemical characterization using FTIR, ^{13}C CP MAS NMR, PXRD, XPS, TGA-MS, SEM, EPR, N_2 physisorption and nitrate content analysis shows that during activation, up to 85 % of the nitrate anions are selectively removed from the structure and replaced with other charge compensating anions such as O^{2-} . The defect sites generated via this activation act as new strong basic sites within the catalyst structure. A fluorescence microscopic visualization of the activity convincingly proves that the activity is exclusively associated with the hexagonal crystals, and that reaction proceeds inside the crystal's interior. Theoretical analysis of the Ba-material shows that the basicity of the proposed $\text{Ba}^{2+}\text{-O}^{2-}\text{-Ba}^{2+}$ motives is close to that of edge sites in BaO.

Introduction

Metal-organic frameworks (MOFs) have attracted much interest due to their large compositional and structural diversity. Numerous applications have been investigated so far, such as gas storage, separations and catalysis.¹⁻³ The exploration of MOFs as catalysts however has mainly focused on acid or redox catalysis. Reports on the catalytic activity of MOFs in base catalyzed reactions are much more scarce, mainly focusing on porous materials containing N-functionalized linkers, e.g. aminoterephthalic acid.⁴⁻⁷ In these materials, the N-functionality acts as the basic catalytic site. The relatively weak basicity of these sites however, with electron withdrawing carboxylic groups on the same aromatic ring, limits the reaction scope of these catalysts. Furthermore, a recent study has shown that the catalytic activity of the amino-substituted Zn-MOF IRMOF-3 can be attributed to defect sites rather than to the amine functionality.⁸ A second, smaller group of basic MOF catalysts comprises structures without micropores or with very narrow micropores, featuring basic sites mainly at lattice terminating surface sites. Examples of such materials are ZIF-8 and ZIF-9,⁹⁻¹¹ in which the pore windows are too narrow to

allow diffusion of most reactants and/or products, or a Ba-3,5-pyrazoledicarboxylate MOF having a limited microporous volume.¹² If catalysis is confined to the outer surface, the catalytic material is used only for a very limited fraction, and the precise nature of the sites at the surface is not always well defined.

Rather than focusing on the linker as a source of basic sites, modification of the inorganic building unit forms an alternative option for creating basicity in MOFs. Metal oxides such as MgO, CaO, SrO and BaO are generally known to be active, industrially applied basic catalysts.^{13, 14} Their activity is attributed to low-coordination sites located on the crystal surface or at corners and edges.^{15, 16} The high dispersion of e.g. metal-oxygen or metal-hydroxide strands in certain alkaline earth metal MOFs may provide a starting point for imparting base catalytic activity to these MOFs. The challenge is then to develop activation procedures that generate uniform, localized defects throughout the structure without causing complete structural decay. With such aim, the present study focuses on the active site formation in the Ba- and Sr-MOFs $M_2(\text{BTC})(\text{NO}_3)(\text{DMF})$ ($M = \text{Ba}$ or Sr , $\text{H}_3\text{BTC} = 1,3,5\text{-}$

benzenetricarboxylic acid, DMF = *N,N*-dimethylformamide). These structures were first reported by Foo et al.¹⁷ and Lee et al.¹⁸ for the Ba- and the Sr-variant respectively, and exhibit some remarkable structural features. Whereas the connectivity of the inorganic building units in most MOFs is of a 0, 1 or 2-dimensional nature, forming inorganic nodes, chains or planes, the M-O-M bonds in these Ba- and Sr-materials extend in 3 dimensions. Such frameworks can therefore be classified as \bar{f}^3O^0 type frameworks according to Cheetham.¹⁹ The inorganic building unit and the trimesate linker combine to form hexagonal prism shaped crystals with large three-leaf-clover-shaped channels running along the length of the crystals in the [001] direction (Fig. 1, top). The pore dimension of each channel is approximately 13 Å at its widest point and 6.5 Å at its narrowest part. Most important in this study however is the presence of nitrate anions in the structure. These anions line the walls of the pores and are required for charge neutrality (Fig. 1, bottom). Here we show that thermal pretreatment of these materials results in the controlled decomposition of the nitrate anions, with formation of $\text{Ba}^{2+}\text{-O}^{2-}\text{-Ba}^{2+}$ motifs along the channels. These provide the material with a high activity in base-catalyzed reactions. Fluorescence microscopy proves that the activity is situated inside the channels of the MOF.

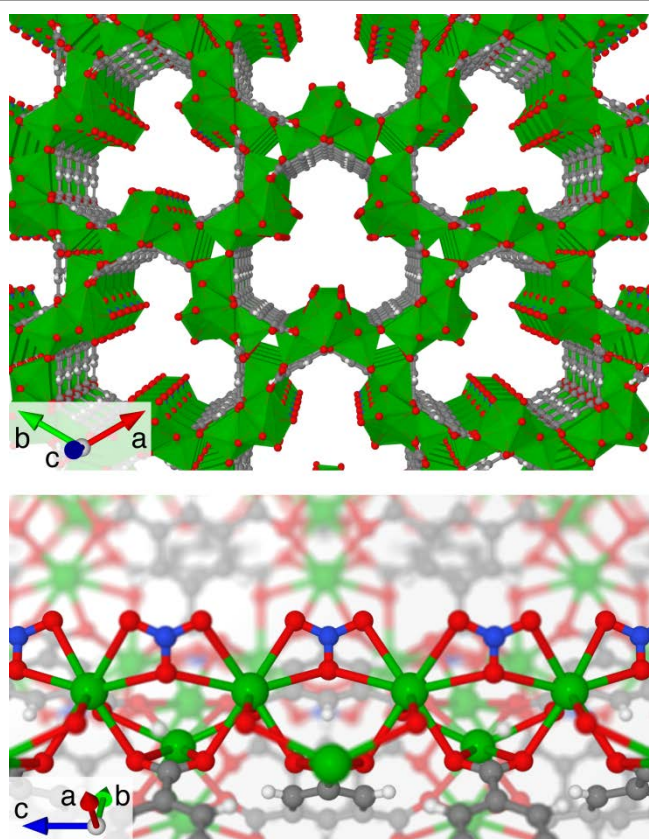


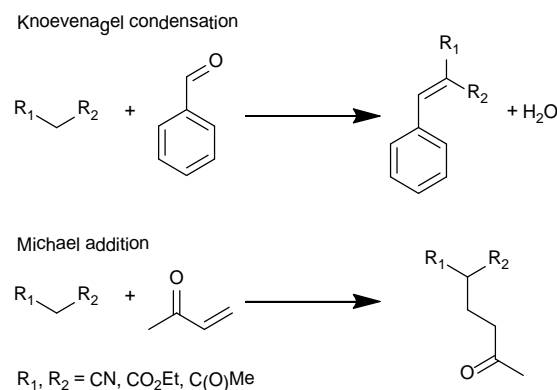
Fig. 1 Pore structure of $\text{Ba}_2(\text{BTC})(\text{NO}_3)$ (top) and close-up of the nitrate chain running lengthwise through the pores of the MOF (bottom). Green, blue, red, grey and white represent barium, nitrogen, oxygen, carbon and hydrogen respectively.

Results and discussion

Catalytic activity of $\text{Ba}_2(\text{BTC})(\text{NO}_3)$ and $\text{Sr}_2(\text{BTC})(\text{NO}_3)$ derived materials

As the interest of the MOF community has often focused on sorption applications, creation of permanent porosity by pore evacuation has been studied in detail for many materials. A highly evacuated state of a material however does not necessarily correspond to the catalytically most active state; hence, the activation procedures for the Ba- and Sr-MOFs were optimized with regard to the catalytic activity rather than aiming for the largest values of the pore volume. The catalytic activities of the Ba- and Sr-MOFs, activated at different temperatures, were evaluated using model Knoevenagel condensation and Michael addition reactions at 70 °C (Scheme 1). Besides the $\text{Ba}_2(\text{BTC})(\text{NO}_3)$ and $\text{Sr}_2(\text{BTC})(\text{NO}_3)$ MOFs, a range of other alkaline earth dicarboxylate MOFs were included in a preliminary activity screening (see supporting information). These activation treatments did not result in any activity increase for most materials studied; however, for $\text{Ba}_2(\text{BTC})(\text{NO}_3)$, an elevated activation temperature was found to produce a remarkably large increase of the catalytic activity in the different reactions (Fig. 2). For instance, with $\text{Ba}_2(\text{BTC})(\text{NO}_3)$, pretreated at 320 °C as the catalyst, the Knoevenagel condensation of malonitrile and benzaldehyde, or the Michael addition of ethyl cyanoacetate on methyl vinyl ketone, proceeded with yields of 99 and 93 % respectively. A similar effect was found for the isostructural Sr-MOF (Fig. 2 inset). In general, the activity of the $\text{Sr}_2(\text{BTC})(\text{NO}_3)$ MOF after activation at 320 °C is somewhat lower than that of the related Ba-material, as illustrated for instance for the Knoevenagel condensation reaction of ethyl cyanoacetate (ECA) and benzaldehyde. For alkaline earth metal oxides, the basic strength is known to decrease in the order $\text{BaO} > \text{SrO} > \text{CaO} > \text{MgO}$.²⁰ The similar activity order of the activated Ba- vs. Sr-MOFs already suggests that the alkaline earth ions are intimately involved in the base catalytic activity.

The reactivity of different donor molecules was investigated using $\text{Ba}_2(\text{BTC})(\text{NO}_3)$ activated overnight at 320 °C as a standard catalyst. Besides malonitrile and ethyl cyanoacetate,



Scheme 1

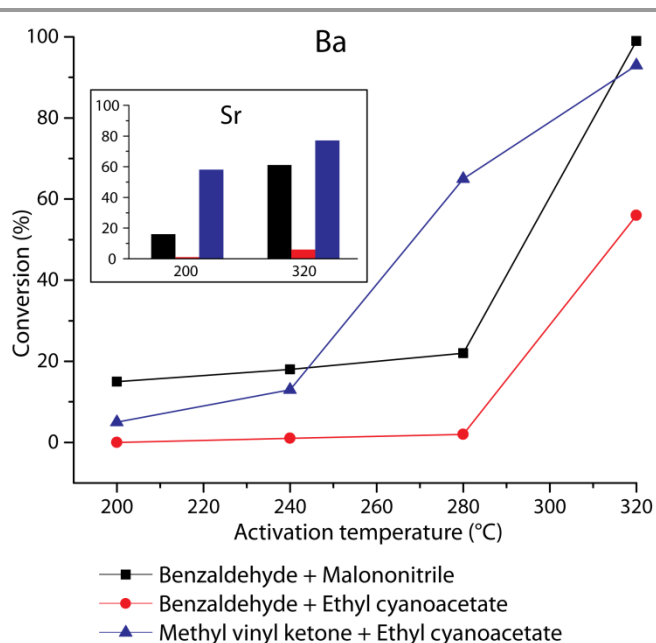


Fig. 2 Conversion of the acceptor molecule observed after 24 h of reaction at 70 °C in Knoevenagel addition and Michael condensation reactions, as a function of the activation temperature for the Ba-MOF and the Sr-MOF (inset).

also ethyl acetoacetate was used in the Knoevenagel condensation with benzaldehyde (Table 1, entries 1-3). Although the reaction temperature was increased from 70°C to 110°C, only limited conversion of ethyl acetoacetate was observed after 24 h compared to the reactions of the more acidic malononitrile or ethyl cyanoacetate donors. This clearly shows that at least for the Knoevenagel condensation reaction, the acidity of the donor molecule strongly determines the overall conversion, as expected for a base catalyzed reaction. Using malononitrile as the donor molecule, the acceptor molecule benzaldehyde can be readily replaced by its functionalized variants, e.g. *p*-bromo- or *p*-nitrobenzaldehyde, without significant loss in conversion (entries 4-7). Acetophenone as an acceptor molecules leads to diminished yields, probably due to steric hinderance (entry 8), whereas the

cyclic ketones cyclopentanone and cyclohexanone show moderate to high conversions (entries 9-10).

For the Michael addition reactions (Table 1, entries 11-15), the correlation between the acidity of the donor molecule and the overall conversion is less straightforward. Even with moderately acidic donors like 2,4-pentanedione or ethyl acetoacetate, excellent conversions are achieved (> 99%; entries 13-14), while conversion of a more acidic reactant like malononitrile is somewhat lower (entry 2). The fact that rates are not only dependent on the acidity of the donor, suggests that in the Michael addition, the Ba₂(BTC)(NO₃) catalyst activates not only the donor molecules, but also the acceptor molecules. Specifically, the α,β-unsaturated carbonyl moiety of methyl vinyl ketone could be activated on the Lewis acid component of the acid-base pair of the active site.²¹ The limited conversion in the reaction of diethyl malonate (entry 15) however illustrates that a too low pK_a may still adversely affect the overall conversion for a Michael donor lacking nitrile functionalities.

Fluorescence microscopy was used to confirm the base catalytic activity of the MOF material (Fig. 3). NASCA ('Nanometer Accuracy by Stochastic Chemical reAction') microscopy films individual catalytic conversions of a non-fluorescent reactant molecule to a strongly fluorescent product molecule, resp. fluorescein diacetate (FDA) and fluorescein in this study.²² There are two major observations: first, the catalytic activity is clearly associated with the hexagonal prism shaped MOF crystals, and not with debris or disintegrated crystals. Secondly, a homogeneous activity was observed throughout the whole crystal. To better confirm the presence of catalytic activity in the center of the MOF particles, confocal imaging with the focal plane located at the center of the crystals was performed. These measurements reveal that transesterification, even of the bulky FDA probe molecules, occurs over the entire volume of the catalyst particle. Moreover, when the onset of fluorescence is monitored by confocal microscopy directly after the addition of FDA, a gradient in fluorescence can be observed along the long axis of the crystals, corresponding to the channels in the [001] direction. As expected, this gradient is due to gradual diffusion of FDA in the pores. Active sites located near the pore

Table 1 Exploration of the substrate scope for the Ba₂(BTC)(NO₃) material activated at 320°C for 16h.^a

	Donor	pK _a (DMSO)	Acceptor	X _{acceptor} -%
1	malononitrile	11.1	Benzaldehyde	97
2	ethyl cyanoacetate	13.1	Benzaldehyde	85
3	ethyl acetoacetate	14.3	Benzaldehyde	6
4	malononitrile	11.1	<i>p</i> -bromobenzaldehyde	92
5	malononitrile	11.1	<i>p</i> -nitrobenzaldehyde	88
6	malononitrile	11.1	<i>o</i> -nitrobenzaldehyde	80
7	malononitrile	11.1	<i>p</i> -methoxybenzaldehyde	72
8	malononitrile	11.1	acetophenone	3
9	malononitrile	11.1	cyclopentanone	29
10	malononitrile	11.1	cyclohexanone	92
11	malononitrile	11.1	methyl vinyl ketone	33
12	ethyl cyanoacetate	13.1	methyl vinyl ketone	77
13	2,4-pentanedione	13.3	methyl vinyl ketone	99
14	ethyl acetoacetate	14.3	methyl vinyl ketone	99
15	diethyl malonate	16.4	methyl vinyl ketone	1

^a Reaction conditions: 1 mmol of each reactant; 2 ml toluene, 110 °C, 50 mg MOF.

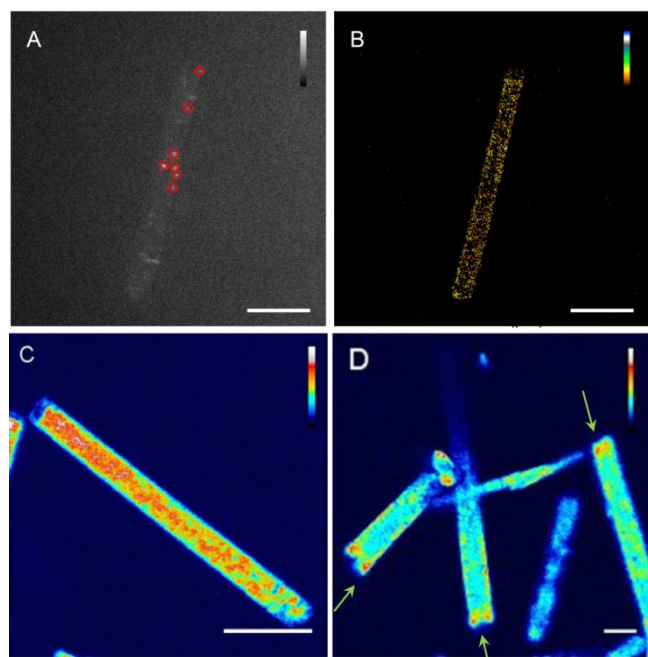


Fig. 3 Fluorescence microscopy on $\text{Ba}_2(\text{BTC})(\text{NO}_3)$. (A) Wide-Field FM image of fluorescein diacetate (FDA; $4.2 \times 10^{-7} \text{M}$) conversion (red circles indicate localized single reaction events); (B), NASCA reactivity map generated by localization of reaction events during 150 seconds; (C) Confocal FM image of the FDA ($1 \times 10^{-4} \text{M}$) conversion; (D) Confocal FM image of the onset of fluorescence soon after introduction of FDA. Green arrows point at local increase of fluorescence in the tips of the crystal. Scale bars for all the images are $5 \mu\text{m}$.

openings are more easily reached by the FDA and display higher catalytic activity reflected in a stronger fluorescence than active sites located near the center of the hexagonal crystals.

Finally, the heterogeneity of the $\text{Ba}_2(\text{BTC})(\text{NO}_3)$ catalyst activated overnight at 320°C was evaluated via a hot filtration test on a Michael addition reaction of ethyl cyanoacetate and methyl vinyl ketone in toluene at 70°C (Fig. S1, supporting information). Removal of the catalyst after 2 h of reaction, confirms that catalysis is indeed fully heterogeneous. Repeated use of the $\text{Ba}_2(\text{BTC})(\text{NO}_3)$ catalyst in consecutive runs of the Knoevenagel condensation of benzaldehyde and malononitrile showed that the catalyst is reusable (Fig. S2), and the catalyst maintained its high activity (99% conversion after 24 h) in the same reaction, after contact with air followed by a mild drying procedure, illustrating that it is not very sensitive towards CO_2 .

Elucidating the effects of the activation procedure

The activity of the tested $\text{Ba}_2(\text{BTC})(\text{NO}_3)$ and $\text{Sr}_2(\text{BTC})(\text{NO}_3)$ materials (as shown in Fig. 2) evidences a large influence of the activation procedure on the catalytic activity. As the largest activity increase was observed for the samples activated at 320°C , this procedure was chosen as a standard for investigating the structural and chemical origins of the increased catalytic activity.

The removal of residual DMF molecules and other species during the activation of the catalyst was monitored in a TGA-

MS experiment. To fully simulate the activation procedure, the TGA of $\text{Ba}_2(\text{BTC})(\text{NO}_3)$ was performed under He-atmosphere and the temperature profile was identical to that of the activation procedure. Three distinct transitions can be observed in the evolution of the ion count with time (Fig. 4). In the first two steps, physisorbed and chemisorbed DMF (73 Da) molecules are released from the framework. At this stage, the rise in intensity of the other mass fragments (30, 44 and 46 Da) is due to further fragmentation of DMF in the mass spectrometer. In the third step centered at 300°C , however, a rise in intensity can be observed for the lighter fragments (30, 44 and 46 Da), but not at all for the 73 Da signal. Hence, these signals correspond to species different from DMF. Given their mass, these are likely NO_x species such as NO, NO_2 and N_2O , produced by decomposition of the nitrate anions which line the pores of the material.

The loss of nitrate anions from the structure may also be observed via spectroscopic techniques such as FTIR and XPS spectroscopy (Fig. 5 A and B respectively). The evolution of the IR absorbance band of nitrate was monitored *in situ* during the activation using a temperature and pressure controlled measuring cell. A loss in absorbance at 822 cm^{-1} is noticed with

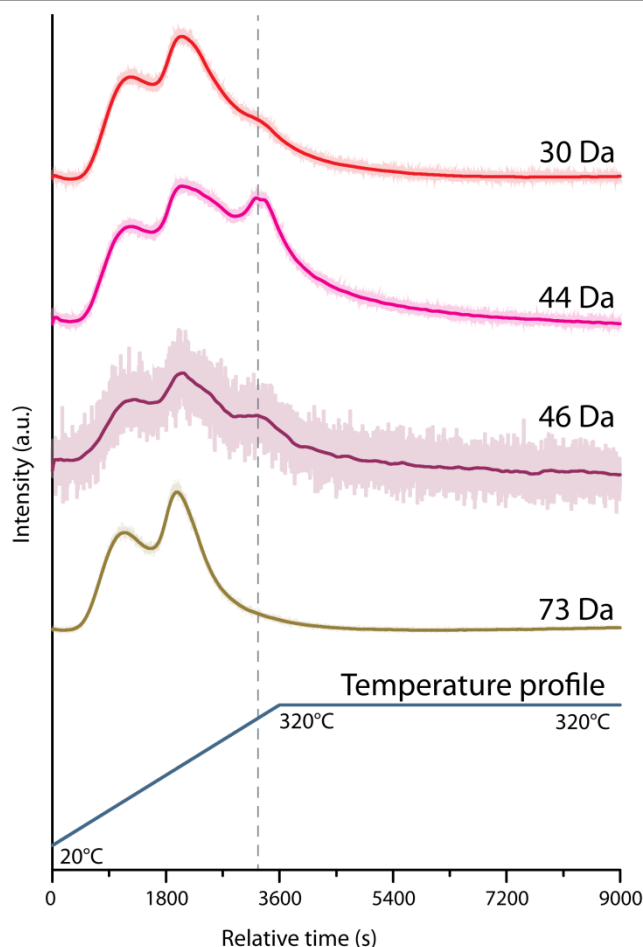


Fig. 4 Time-dependent evolution of different mass fragments in gases produced by thermal activation of $\text{Ba}_2(\text{BTC})(\text{NO}_3)(\text{DMF})$ as observed via TGA-MS. The event at 300°C corresponds to the decomposition of structure-embedded nitrate.

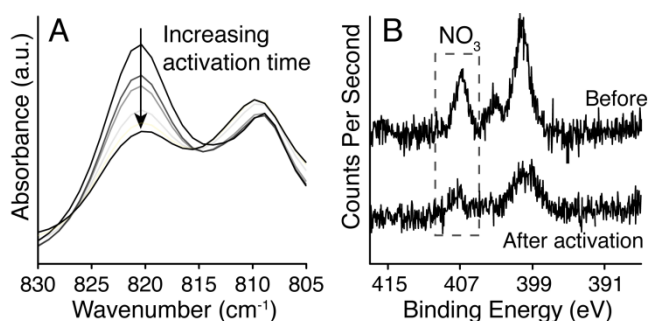
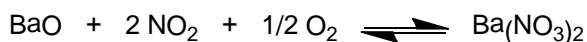


Fig. 5 Evolution of the FTIR (A) and XPS spectra (B) of the nitrate species upon activation of $\text{Ba}_2(\text{BTC})(\text{NO}_3)$.

increasing activation time. Pure $\text{Ba}(\text{NO}_3)_2$ salt exhibits an absorbance band at 817 cm^{-1} .²³ By exchanging the DMF solvent coordinated in the pores for MeOH, the presence of this absorbance band was found to be independent from the coordinating solvent and therefore it can unambiguously be attributed to the nitrate anions. In XPS, the N1s signal of nitrate can be found at 407 eV. Comparison of the signal intensities of the pristine and the activated material, using the Ba3d signal at 779 eV as an internal standard, a very substantial loss of at least 70 % in nitrate was observed.

Finally, the loss of nitrate anions was unambiguously proven by measurement of the nitrate and metal contents of the materials before and after activation. The nitrate content of the material can be accurately determined after dissolution of the material using a colorimetric assay whereas the metal content was measured from the solution using ICP-MS. Prior to activation, the experimental $\text{NO}_3:\text{Ba}$ -ratio was 0.57, which agrees rather well with the theoretically expected ratio of 0.5. After activation however, the $\text{NO}_3:\text{Ba}$ -ratio dropped to 0.08, corresponding to a loss in nitrate content of approximately 85%. Such a thermally induced decomposition of Ba-associated nitrate is actually well known and is used in practice in e.g. NO_x Storage and Reduction (NSR) systems for the reduction of NO_x -emissions from lean-burn power sources.²⁴ Although the full mechanism is complex, NO_x is reversibly stored and released on BaO in these systems according to equilibrium reactions such as:



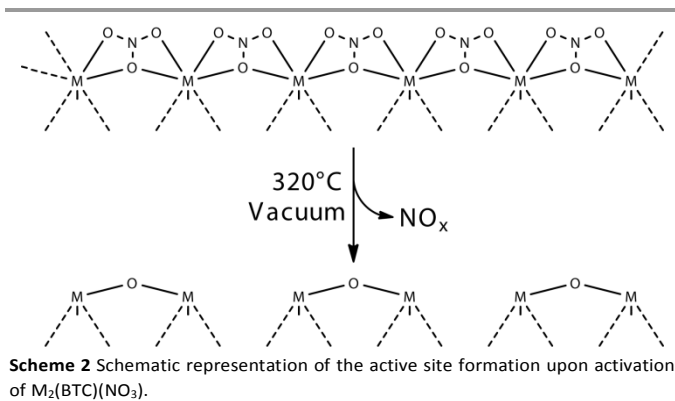
Both temperature and (partial) pressure are important driving forces for the conversion of nitrates back to oxides. Increasing the temperature as well as reducing the partial pressure of oxygen dramatically reduces the stability of nitrate species. Furthermore, the decomposition of barium nitrate under vacuum is reported to occur at temperatures as low as $200\text{ }^\circ\text{C}$.²⁵ Hence, the perfect match between the available literature data on $\text{Ba}(\text{NO}_3)_2$ decomposition and the observation of the gaseous decomposition products during TGA-MS on $\text{Ba}_2(\text{BTC})(\text{NO}_3)$, strongly suggests the transformation of two MOF-embedded nitrate anions into one, surface-bound O^{2-} -anion.

The chemical stability of the linker molecules in the MOF when exposed to the activation procedure was evaluated using solid

state ^{13}C CP MAS NMR (Fig. S3). As the activation time increases, the removal of the DMF molecules from the framework is apparent from the loss in intensity of the signals at 31, 37 and 166 ppm in the spectra. The signals at 134, 136 and 178 ppm, corresponding to the aromatic and carboxylic carbon atoms of trimesate, are preserved regardless of the duration of the activation procedure, indicating the integrity of the linker molecules in the framework. Broadening of the signals, which becomes more apparent with longer activation procedure, can be attributed to local disorder and symmetry losses in the crystal structure.

The structural changes induced by the activation procedure were studied by monitoring the crystallinity, the texture and the particle morphology using powder X-ray diffraction (PXRD), nitrogen physisorption and scanning electron microscopy respectively. X-ray diffractograms recorded before and after activation (Fig. S4) show a decrease in crystallinity of the material. This is most likely due to the decomposition of the surface bound nitrate anions which induces stress in the parent framework; relaxation of the material will result in a loss of long range order and crystallinity. This observation is supported by the periodic PBE-D3 optimizations indicating a volume expansion of 4% in case of the unit cell containing a defect site (see supporting information). However, both for the Ba and Sr based materials, the major reflections at low angles can still very clearly be observed. This is in good agreement with the peak widening observed in the solid state NMR measurements of the activated samples. The relaxation of the materials however does not result in a complete deterioration of the material. Nitrogen physisorption measurements show a good retention of the microporosity upon activation at $320\text{ }^\circ\text{C}$ for $\text{Sr}_2(\text{BTC})(\text{NO}_3)$ (Fig. S5), with an increase in BET surface area from $560\text{ m}^2/\text{g}$ to $680\text{ m}^2/\text{g}$. Electron micrographs (Fig. S6) indicate that there is a good retention of the particle morphology. Locally, signs of cracking and flaking of the material can be observed. This may further improve the catalytic activity of the material as it shortens the diffusion pathways for the reactant molecules, which run lengthwise through the particles.

When combining the information gathered from various physicochemical techniques, the increased activity of $\text{Ba}_2(\text{BTC})(\text{NO}_3)$ and $\text{Sr}_2(\text{BTC})(\text{NO}_3)$ upon activation at high temperatures can be related to the selective decomposition of one type of anions, viz. the structural nitrate anions. These nitrate ions line the pore walls and are important for the overall charge balance within the material (Fig. 1, bottom). As these anions are lost, charge neutrality can only be maintained by O^{2-} ions which are introduced in the structure by the decomposition of nitrate (Scheme 2). Hence, the MOF with a structure formula $\text{Ba}_2(\text{BTC})(\text{NO}_3)(\text{DMF})_x$ is converted into an active catalyst with an approximate structure formula $\text{Ba}_2(\text{BTC})(\text{NO}_3)_{0.15}(\text{O})_{0.425}$. As two nitrate anions are replaced by one O^{2-} -anion, multiple low-coordination metal sites are generated throughout the framework. These low-coordination metal ions, combined with the bridging O^{2-} -anions can thus be viewed as a new type of active sites, explaining the overall catalytic activity of the



materials. The formed $\text{Ba}^{2+}\text{-O}^{2-}\text{-Ba}^{2+}$ motifs are highly reminiscent of the low-coordination sites found in alkaline earth oxides, but now nearly all Ba^{2+} -oxide units are available as active sites.

Additional evidence for the generation of such low-coordinated Ba or Sr sites comes from the observation of superoxide ions with electron paramagnetic resonance (EPR, Fig. 6). Prior to activation, no superoxide signals could be detected in the EPR spectra of the Sr- and Ba-MOFs. After activation at 320°C however, the new electron rich active sites, generated during activation, can interact with molecular oxygen, generating superoxide ions which are clearly visible in the spectra of both the Sr- and the Ba-MOFs. The g parameters from a fit are $g_{\parallel} = 2.087$ and $g_{\perp} = 2.005$ for activated $\text{Ba}_2(\text{BTC})(\text{NO}_3)$; $g_{\parallel} = 2.079$ and $g_{\perp} = 2.006$ for $\text{Sr}_2(\text{BTC})(\text{NO}_3)$. Such values are highly characteristic for surface bound superoxide anions.^{26, 27}

Finally, the basicity of the newly generated active site was compared with that of the original nitrate rich material using proton affinities (PAs) calculated via DFT-based simulations as a measure for the basicity.^{28, 29} Fig. 7 shows that the PA value of the Ba-MOF cluster increases substantially upon transformation of the nitrate anions. In particular, when a defect site ($-\text{Ba}[\ast]-\text{Ba}-\text{O}-$) is generated in the model, the computed PA value increases from 876 to 1153 kJ/mol. This effect is even more pronounced when a defect site is combined with a residual NO_3 unit: in that case, the computed PA value increases from 876 to 1233 kJ/mol. This increase in PA corresponds with an increase in basicity, and hence the theoretical analysis supports the observation that introduction of a defect site results in an increased basic character. To get insight into the strength of the newly generated basic sites, a comparison with the prototype basic material cubic BaO was made. The PA values of a $(\text{BaO})_{16}$ cluster show that the basicity of the newly generated active site is similar to that of the metal oxide cluster, which gives solid evidence for the basicity of the O^{2-} defect sites generated here.

Conclusions

Summarizing, the Sr- and Ba-MOFs $M_2(\text{BTC})(\text{NO}_3)(\text{DMF})$ were shown to be active base catalysts in different Knoevenagel condensation and Michael addition reactions. The catalytic

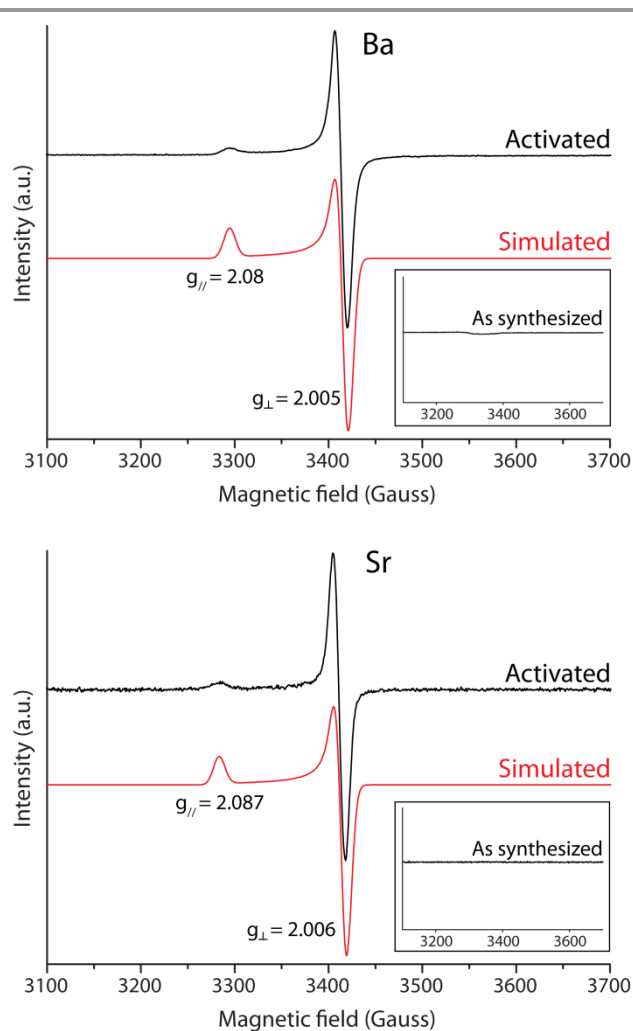


Fig. 6 EPR spectra of the Ba (above) and Sr (below) $M_2(\text{BTC})(\text{NO}_3)$ after 16 h of activation at 320°C compared with the simulated spectra. Inset: spectra of the samples before activation.

activity could be markedly increased via a vacuum pretreatment procedure at 320°C . This is the result of a loss of nitrate ions from the framework and the concomitant generation of new active sites consisting of low-coordination metal ions and O^{2-} -anions. Theoretical analysis of the Ba-material shows that the basicity of the proposed $\text{Ba}^{2+}\text{-O}^{2-}\text{-Ba}^{2+}$ motives is close to that of edge sites in BaO. This clearly illustrates that the discovery of new activation procedures is indispensable for the further development of MOFs as catalysts.

Acknowledgements

The authors are grateful to the Belgian Federal Government for support in the IAP project 07/05 Functional Supramolecular Systems, to KU Leuven for the Methusalem CASAS grant, and to FWO Vlaanderen for research project funding G.0453.09 and G.0486.12. P.V., T.D.B., M.V. and K.H. are grateful for a fellowship from FWO Vlaanderen. Funding was also obtained from the Research Board of Ghent University (BOF) and from the European Research Council under the European

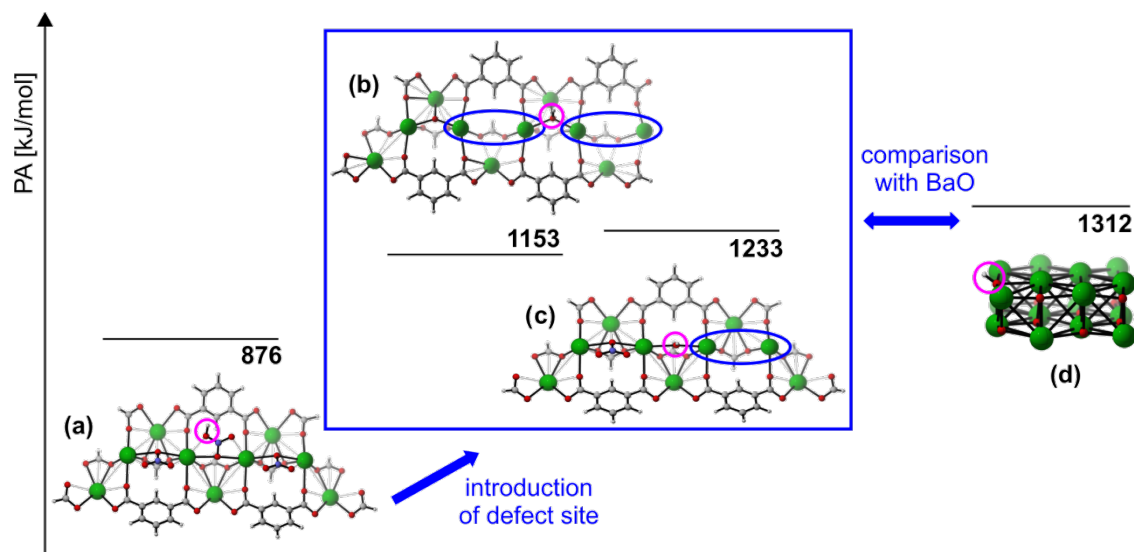


Fig. 7 Theoretical proton affinities of optimized Ba-MOF clusters: (a) the original cluster containing NO_3 units, (b) cluster representing a defect site and (c) cluster containing a defect site as well as a NO_3 unit. Computed PA value of optimized $(\text{BaO})_{16}$ cluster (d) is also included. Values in kJ/mol and calculated using B3LYP/6-311G(d,p) and def2-tzvp, see computational methods. Protonated structures are depicted, the position of the proton is indicated with a pink circle.

Community's Seventh Framework Programme (FP7(2007-2013) ERC grant agreement number 240483). MBRJ acknowledges the European Research Council for financial support (ERC Starting Grant 307523) and the "Fonds voor Wetenschappelijk Onderzoek" (Grants G0197.11, G.0962.13). The authors would also like to thank Dirk Dom for performing the EPR measurements, Nico De Roo for performing the XPS measurements, Peter Salaets for performing the nitrate analysis and Kristin Coorevits for the elemental analysis.

Notes and references

^a Centre for Surface Chemistry and Catalysis, KU Leuven - University of Leuven, Kasteelpark Arenberg 23, box 2461, 3001 Leuven, Belgium.

^b Center for Molecular Modeling, Universiteit Gent, Technologiepark 903, 9052 Zwijnaarde, Belgium.

^c Department of Earth and Environmental Sciences, KU Leuven - University of Leuven, Kasteelpark Arenberg 20, 3001 Leuven, Belgium.

^d Department of Solid State Chemistry, Universiteit Gent, Krijgslaan 281 S1, 9000 Ghent, Belgium.

* Corresponding author: dirk.devos@biw.kuleuven.be

Electronic Supplementary Information (ESI) available: additional figures, experimental procedures, catalytic data on other alkaline earth metal MOFs, mass spectra of reaction products, details on the theoretical modelling. See DOI: 10.1039/b000000x/

- 1 J. R. Li, J. Sculley and H. C. Zhou, *Chem. Rev.*, 2012, **112**, 869-932.
- 2 A. Corma, H. García and F. X. Llabrés i Xamena, *Chem. Rev.*, 2010, **110**, 4606-4655.
- 3 P. Valvekens, F. Vermoortele and D. De Vos, *Catal. Sci. Technol.*, 2013, **3**, 1435-1445.
- 4 J. Gascon, U. Aktay, M. D. Hernandez-Alonso, G. P. M. van Klink and F. Kapteijn, *J. Catal.*, 2009, **261**, 75-87.

- 5 P. Kasinathan, Y. K. Seo, K. E. Shim, Y. K. Hwang, U. H. Lee, D. W. Hwang, D. Y. Hong, S. B. Halligudi and J. S. Chang, *Bull. Korean Chem. Soc.*, 2011, **32**, 2073-2075.
- 6 M. Savonnet, S. Aguado, U. Ravon, D. Bazer-Bachi, V. Lecocq, N. Bats, C. Pinel and D. Farrusseng, *Green Chem.*, 2009, **11**, 1729-1732.
- 7 Y. Tan, Z. Fu and J. Zhang, *Inorganic Chemistry Communications*, 2011, **14**, 1966-1970.
- 8 F. X. Llabrés i Xamena, F. G. Cirujano and A. Corma, *Microporous Mesoporous Mater.*, 2012, **157**, 112-117.
- 9 U. P. N. Tran, K. K. A. Le and N. T. S. Phan, *ACS Catal.*, 2011, **1**, 120-127.
- 10 C. Chizallet, S. Lazare, D. Bazer-Bachi, F. Bonnier, V. Lecocq, E. Soyer, A. A. Quoineaud and N. Bats, *J. Am. Chem. Soc.*, 2010, **132**, 12365-12377.
- 11 L. T. L. Nguyen, K. K. A. Le, H. X. Truong and N. T. S. Phan, *Catal. Sci. Technol.*, 2012, **2**, 521-528.
- 12 T. Maity, D. Saha, S. Das and S. Koner, *Eur. J. Inorg. Chem.*, 2012, **2012**, 4914-4920.
- 13 H. Hattori, *Chem. Rev.*, 1995, **95**, 537-558.
- 14 K. Tanabe and W. F. Hölderich, *Appl. Catal.*, A, 1999, **181**, 399-434.
- 15 S. Coluccia, A. Barton and A. J. Tench, *J Chem Soc Faraday T 1*, 1981, **77**, 2203-2207.
- 16 S. Coluccia, A. J. Tench and R. L. Segall, *J Chem Soc Faraday T 1*, 1979, **75**, 1769-1779.
- 17 M. L. Foo, S. Horike, Y. Inubushi and S. Kitagawa, *Angew. Chem., Int. Ed.*, 2012, **51**, 6107-6111.
- 18 D. W. Lee, V. Jo and K. M. Ok, *Cryst. Growth Des.*, 2011, **11**, 2698-2701.
- 19 A. K. Cheetham, C. N. R. Rao and R. K. Feller, *Chem. Commun.*, 2006, 4780-4795.
- 20 K. Tanabe and K. Saito, *J. Catal.*, 1974, **35**, 247-255.
- 21 S. Bhaduri and D. Mukesh, *Homogeneous Catalysis: Mechanisms and Industrial Applications*, John Wiley & Sons, Inc., 2002.

- 22 M. B. J. Roeffaers, G. De Cremer, J. Libeert, R. Ameloot, P. Dedecker, A.-J. Bons, M. Bueckins, J. A. Martens, B. F. Sels, D. E. De Vos and J. Hofkens, *Angew. Chem.-Int. Edit.*, 2009, **48**, 9285-9289.
- 23 SDBSWeb: <http://sdbs.riondb.aist.go.jp> (National Institute of Advanced Industrial Science and Technology 15/10/2013).
- 24 W. S. Epling, L. E. Campbell, A. Yezerets, N. W. Currier and J. E. Parks, *Cataly Rev*, 2004, **46**, 163-245.
- 25 Y. S. Sayi, C. S. Yadav, P. S. Shankaran, G. C. Chhapru, K. L. Ramakumar and V. Venugopal, *Int. J. Mass Spectrom.*, 2002, **214**, 375-381.
- 26 M. Chiesa, E. Giamello and M. Che, *Chem. Rev.*, 2010, **110**, 1320-1347.
- 27 M. Anpo, M. Che, B. Fubini, E. Garrone, E. Giamello and M. Paganini, *Top. Catal.*, 1999, **8**, 189-198.
- 28 R. Cortese and D. Duca, *Phys. Chem. Chem. Phys.*, 2011, **13**, 15995-16004.
- 29 P. Valvekens, M. Vandichel, M. Waroquier, V. Van Speybroeck and D. De Vos, *J. Catal.*, 2014, **317**, 1-10.